Article

Kinetically Controlled Catalytic Formation of Zinc Oxide Thin Films at Low Temperature

David Kisailus, Birgit Schwenzer, John Gomm, James C. Weaver, and Daniel E. Morse

J. Am. Chem. Soc., **2006**, 128 (31), 10276-10280• DOI: 10.1021/ja062434l • Publication Date (Web): 18 July 2006

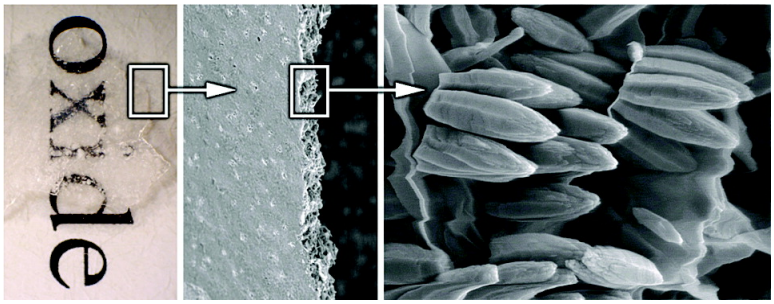

J|A|C|S
ARTICLES
Published on Web 07/18/2006

Kinetically Controlled Catalytic Formation of Zinc Oxide Thin Films at Low Temperature

David Kisailus,[†,‡,§] Birgit Schwenzer,[‡,§] John Gomm,[‡,§] James C. Weaver,[‡,§] and Daniel E. Morse*[,‡,§,||]

Contribution from HRL Labs LLC, 3011 Malibu Canyon Road, Malibu, California 90265, Institute for Collaborative Biotechnologies, Materials Research Laboratory and the California NanoSystems Institute, Department of Molecular, Cellular, and Developmental Biology, University of California, Santa Barbara, California 93106-9610

Received April 21, 2006; E-mail: d_morse@lifesci.ucsb.edu

Abstract: We developed a unique method to produce ZnO thin films by kinetically controlled catalytic hydrolysis of a molecular precursor at low temperature, operating in conjunction with the vectorial control of crystal growth. Using a system in which the diffusion of a volatile catalyst into a solution of molecular precursor of the metal oxide limits the rate of hydrolysis and establishes a gradient of catalyst concentration, we investigated the nucleation of textured nanoparticles at the gas−liquid interface and characterized their subsequent growth. Use of this slow diffusion method combined with prediction of molecular species using a partial charge model enables a higher level of organizational control than obtained in other low-temperature synthesis methods, without the use of organic molecules. Various metal oxides and their morphologies and chemical compositions can be tailored for specific applications using this relatively simple approach.

Introduction

In nature, various organisms have evolved specific control mechanisms to regulate the synthesis of a great diversity of inorganic structures that serve a wide range of biological functions. These biomineralizing species use precise spatial, chemical, and structural control to form complex structures.[1−4] The remarkable mechanical, optical, and ultrastructural properties of the resulting organic−inorganic biocomposites make them particularly attractive to researchers involved in the development of novel environmentally benign synthetic routes to high-performance materials.[1,5−8] We recently discovered that silica formation in a marine sponge is mediated by protein filaments that serve as both catalysts and templates for the biosynthesis and deposition of the mineral.[9−14] These catalytic and structure-directing mechanisms have since been adapted for the kinetically controlled synthesis of a wide range of metal oxide semiconductors including titanium dioxide[10] and gallium oxide.[15] Analysis of the molecular mechanisms responsible for these syntheses[9] and confirmation through the synthesis of catalytic self-assembling peptides and self-assembled monolayers[16−18] revealed that the biomolecular control of crystal nucleation, polymorph, and growth in these systems is the result of the slow catalysis of mineral formation from molecular precursors operating in conjunction with vectorial control of crystal growth exerted by the templates.[19] This in turn led to the development of a biologically inspired approach to synthesis that captures these principles without the use of organic templates or other molecules.[19] We employed that approach using the diffusion of ammonia vapor through the surface of a solution of a molecular precursor of zinc oxide to slowly catalyze the formation of the oxide at low temperature and

[†] HRL Labs LLC.
[‡] Institute for Collaborative Biotechnologies, University of California.
[§] Materials Research Laboratory and the California NanoSystems Institute, University of California.
[||] Department of Molecular, Cellular, and Developmental Biology, University of California.

(1) Heuer, A. H.; Fink, D. J.; Laraia, V. J.; Arias, J. L.; Calvert, P. D.; Kendall, K.; Messing, G. L.; Blackwell, J.; Rieke, P. C.; Thompson, D. H.; Wheeler, A. P.; Veis, A.; Caplan, A. I. *Science* **1992**, *255*, 1098.
(2) Mann, S. *Nature* **1998**, *332*, 119.
(3) Weiner, S.; Addadi, L. *J. Mater. Chem.* **1997**, *7*, 689.
(4) Lowenstam, H. A.; Weiner, S. *On Biomineralization*; Oxford University Press: New York, 1989.
(5) Aizenberg, J.; Tkachenko, A.; Weiner, S.; Addadi, L.; Hendler, G. *Nature* **2001**, *412*, 819.
(6) Sundar, V. C.; Yablon, A. D.; Grazul, J. L.; Ilan, M.; Aizenberg, J. *Nature* **2003**, *424*, 899.
(7) Yang, S.; Chen, G.; Megens, M.; Ullal, C. K.; Han, Y. J.; Rapaport, R.; Thomas, E. L.; Aizenberg, J. *Adv. Mater.* **2005**, *17*, 435.
(8) Aizenberg, J.; Weaver, J. C.; Thanawala, M. S.; Sundar, V. C.; Morse, D. E.; Fratzl, P. *Science* **2005**, *309*, 275.
(9) Zhou, Y.; Shimizu, K.; Cha, J. N.; Stucky, G. D.; Morse, D. E. *Angew. Chem., Int. Ed.* **1999**, *38*, 779.
(10) Sumerel, J. L.; Yang, W.; Kisailus, D.; Weaver, J. C.; Morse, D. E. *Chem. Mater.* **2003**, *15*, 4804.
(11) Shimizu, K.; Cha, J.; Stucky, G. D.; Morse, D. E. *Proc. Natl. Acad. Sci.* **1998**, *95*, 6234.
(12) Morse, D. E. *Trends Biotechnol.* **1999**, *17*, 230.
(13) Cha, J.; Shimizu, K.; Zhou, Y.; Christiansen, S. C.; Chmelka, B. F.; Stucky, G. D.; Morse, D. E. *Proc. Natl. Acad. Sci.* **1999**, *96*, 361.
(14) Morse, D. E. In *The Chemistry of Organic Silicon Compounds*; Apeloig, Y., Ed.; John Wiley and Sons: New York, 2001; Vol. 3, p 805.
(15) Kisailus, D.; Choi, J. H.; Weaver, J. C.; Yang, W.; Morse, D. E. *Adv. Mater.* **2005**, *17*, 314.
(16) Cha, J.; Stucky, G. D.; Morse, D. E.; Deming, T. J. *Nature* **2000**, *403*, 289.
(17) Kisailus, D.; Najarian, M.; Weaver, J. C.; Morse, D. E. *Adv. Mater.* **2005**, *17*, 1234.
(18) Kisailus, D.; Truong, Q.; Amemiya, Y.; Weaver, J. C.; Morse, D. E. *Proc. Natl. Acad. Sci.* **2006**, *103*, 5652.
(19) Schwenzer, B.; Roth, K. M.; Gomm, J. R.; Murr, M.; Morse, D. E. *J. Mater. Chem.* **2005**, *16*, 401.

10.1021/ja062434l CCC: $33.50

vectorially regulate the growth of nanostructured thin films of this electronically important semiconductor.

Zinc oxide, ZnO, is a II−VI semiconducting material (E_g = 3.37 eV) with a relatively high exciton binding energy (60 meV). The electrical, optical, and chemical properties of ZnO intimately depend on its dimension, morphology, and crystallinity,[20] and therefore, this material serves a wide variety of technological applications.[21] ZnO nanostructures have been synthesized by a number of high-temperature methods including chemical vapor deposition (CVD),[22,23] molecular beam epitaxy (MBE),[24] and laser ablation,[25] all of which require costly equipment and a crystalline template. Hydrothermal synthesis,[26,27] sol−gel processing,[28,29] electrodeposition,[30] and other solution-based methods[31−33] are examples of some of the many low-temperature methods developed to reduce the cost of synthesis. In addition, a few bioinspired routes to ZnO that use templates to direct nucleation and growth have been described.[34−36]

Schwenzer et al. recently described a low-temperature, template-free route to the synthesis of crystalline metal hydroxide, oxide, and phosphate films using a vapor diffusion-based solution method.[19] In this approach, an aqueous solution of metal-containing precursor is exposed to a saturated atmosphere of ammonia in a closed chamber. In the simplest use of this method, exposure of the precursor solution to the ammonia vapor induces formation of a crystalline metal hydroxide film at the gas−liquid interface. Schwenzer et al. reported the formation of $Zn_5(OH)_8(NO_3)_2{\cdot}2H_2O$ from an aqueous solution of $Zn(NO_3)_2$.[19] The same precursor solutions are used here to access a novel synthetic pathway to ZnO. The difference in product formation, compared to our previous findings, can be explained by differences in the reaction conditions. In the study reported here, we derive further inspiration from biological systems that produce crystalline minerals. In these systems, the precise control of supersaturation (ultimately dictated by the rate of cation/anion diffusion into spatially constrained and protected spaces) in conjunction with anisotropic structuring of the crystallization environment contribute to the growth of elaborate single-crystalline structures.[37] In our study, lower concentrations of all starting materials were used and the overall reaction times for film formation were longer with the resulting kinetic control favoring the synthesis of highly textured ZnO films. We observe nucleation and growth of ZnO controlled by the local variation in the chemical potential of Zn^{2+} resulting from accumulation of OH^- at the gas−liquid interface. Identification and control of these phenomena can enhance the usefulness of such low-temperature synthetic routes to ZnO and other important optoelectronic materials.

Experimental Section

Synthesis of ZnO by Vapor Diffusion. A 50 mM aqueous solution of zinc nitrate, $Zn(NO_3)_2$ (Alfa Aesar, Ward Hill, MA) contained in a plastic vial, was placed in a desiccator containing a solution of dilute (0.28 wt %) ammonia (Fisher Scientific, Hampton, NH). The desiccator was sealed for 24 h to permit ammonia diffusion into the zinc nitrate solution to initiate hydrolysis. After 24 h the desiccator was then opened and a product film, which had formed at the gas−liquid interface, was removed and washed 5 times with Milli-Q (Millipore) purified (MQ) water to remove unreacted zinc nitrate. Product films were then dried at room temperature for 24 h.

Scanning Electron Microscopy (SEM). Surface features of films were imaged by a cold cathode field-emission scanning electron microscope (SEM; JEOL JSM 6300F, Peabody, MA). Specimens were mounted on conductive carbon adhesive tabs (Ted Pella, Inc., Redding, CA) and examined at 5 kV after gold/palladium sputter coating.

X-ray Diffraction (XRD). Approximately 5 mg of sample was ground to a fine powder and placed on a single-crystal (100) silicon wafer for characterization by X-ray diffraction (Phillips X′Pert; Amsterdam, Netherlands) using a gonio scan (20−60°, 0.02 deg/step, 5 s/step; slits sizes of 0.25, 0.5, 0.25, and 0.2 mm from source to detector).

Transmission Electron Microscopy (TEM). Crushed films were dispersed by sonication in water to form a suspension. TEM specimens were prepared by pipetting a small amount (~20 μL) of the suspension onto holey carbon copper grids (Ted Pella, Inc., Redding, CA). Grids were then dried at room temperature and imaged with a transmission electron microscope (TEM, FEI T-20) to observe film morphologies and obtain structural information via selected area electron diffraction and lattice imaging. Samples were imaged at 200 kV using magnifications from 20 000× to 600 000×. Selected area electron diffraction patterns (SADP) were obtained at camera distances of 55, 83, and 100 cm. A standard evaporated aluminum film (lattice constant = 0.4041 nm) was used as a standard for calibration of the camera.

Results and Discussion

As-prepared films, rinsed and dried, were examined by SEM. Figure 1a depicts thick (ca. 3 μm) films formed by hydrolysis and condensation reactions of the zinc nitrate precursor. Closer examination of the top side of the film reveals smooth, platelike structures (Figure 1b) that cover the surface. Higher magnification imaging reveals anisotropic particles on the underside of the film (Figure 1c).

XRD (Figure 2) confirms that the product synthesized at room temperature by this diffusion-controlled growth process is wurtzite-ZnO (JCPDS# 36-1451; S. G. $P6_3mc$; a = 3.250 Å, c = 5.205 Å).

TEM of the platelike structures (located on the upper surface of the film; Figure 3a) reveals a seed-like core surrounded by fractal outgrowths. SADP of these plates (upper right, Figure 3a) confirms a highly textured, crystalline ZnO film. High-resolution TEM (HR-TEM, Figure 3b) shows the core to be comprised of nanocrystals of ZnO aligned along the c axis [0001] with texturing in the transverse plane of the film. The d spacings of nanocrystals were measured at 2.82 ± 0.03 Å,

(20) Xia, Y.; Yang, P.; Sun, Y.; Wu, Y.; Mayers, B.; Gates, B.; Yin, Y.; Kim, F.; Yan, H. *Adv. Mater.* **2003**, *15*, 353.
(21) Look, D. C. *Mater. Sci. Eng.* **2001**, *B80*, 383.
(22) Huang, M. H.; Wu, Y.; Feick, H.; Tran, N.; Weber, E.; Yang, P. *Adv. Mater.* **2001**, *13*, 113.
(23) Wu, J. J.; Liu, S. C. *Adv. Mater.* **2002**, *14*, 215.
(24) Heo, Y. W.; Varadarajan, V.; Kaufman, M.; Kim, K.; Norton, D. P.; Ren, F.; Fleming, P. H. *App. Phys. Lett.* **2002**, *81*, 3046.
(25) Choi, J. H.; Tabata, H.; Kawai, T. *J. Cryst. Growth* **2001**, *226*, 493.
(26) Andeen, D.; Loeffler, L.; Padture, N.; Lange, F. F. *J. Cryst. Growth* **2003**, *259*, 103.
(27) Cheng, B.; Samulski, E. T. *Chem. Commun.* **2004**, *8*, 986.
(28) Ryu, H. W.; Park, B. S.; Akbar, S. A.; Lee, W. S.; Hong, K. J.; Seo, Y. J.; Shin, D. C.; Park, J. S.; Choi, G. P. *Sens. Actuators B: Chem.* **2003**, *96*, 717.
(29) Wessler, B.; Steinecker, A.; Mader, W. *J. Cryst. Growth* **2002**, *242*, 283.
(30) Yoshida, T.; Komatsu, D.; Shimokawa, N.; Minoura, H. *Thin Solid Films* **2004**, *451−452*, 166.
(31) Vayssieres, L. *Adv. Mater.* **2003**, *15*, 464.
(32) Wang, Z.; Qian, X. F.; Yin, J.; Zhu, Z. K. *Langmuir* **2004**, *20*, 3441.
(33) Govender, K.; Boyle, D. S.; Kenway, P. B.; O'Brien, P. *J. Mater. Chem.* **2004**, *14*, 2575.
(34) Tian, Z. R.; Voigt, J. A.; Liu, J.; McKenzie, B.; McDermott, M. J.; Rodriguez, M. A.; Konishi, H.; Xu, H. *Nat. Mater.* **2003**, *2*, 821.
(35) Gerstel, P.; Hoffmann, R. C.; Lipowsky, P.; Jeurgens, L. P. H.; Bill, J.; Aldinger, F. *Chem. Mater.* **2005**, *18*, 179.
(36) Bauermann, L. P.; Bill, J.; Aldinger, F. *J. Phys Chem. B* **2006**, *110*, 5182.
(37) Schaeffer, T. E.; Ionescu-Zanetti, C.; Proksch, R.; Fritz, M.; Walters, D. A.; Almqvist, N.; Zaremba, C. M.; Belcher, A. M.; Smith, B. L.; Stucky, G. D.; Morse, D. E.; Hansma, P. K. *Chem. Mater.* **1997**, *9*, 1731.

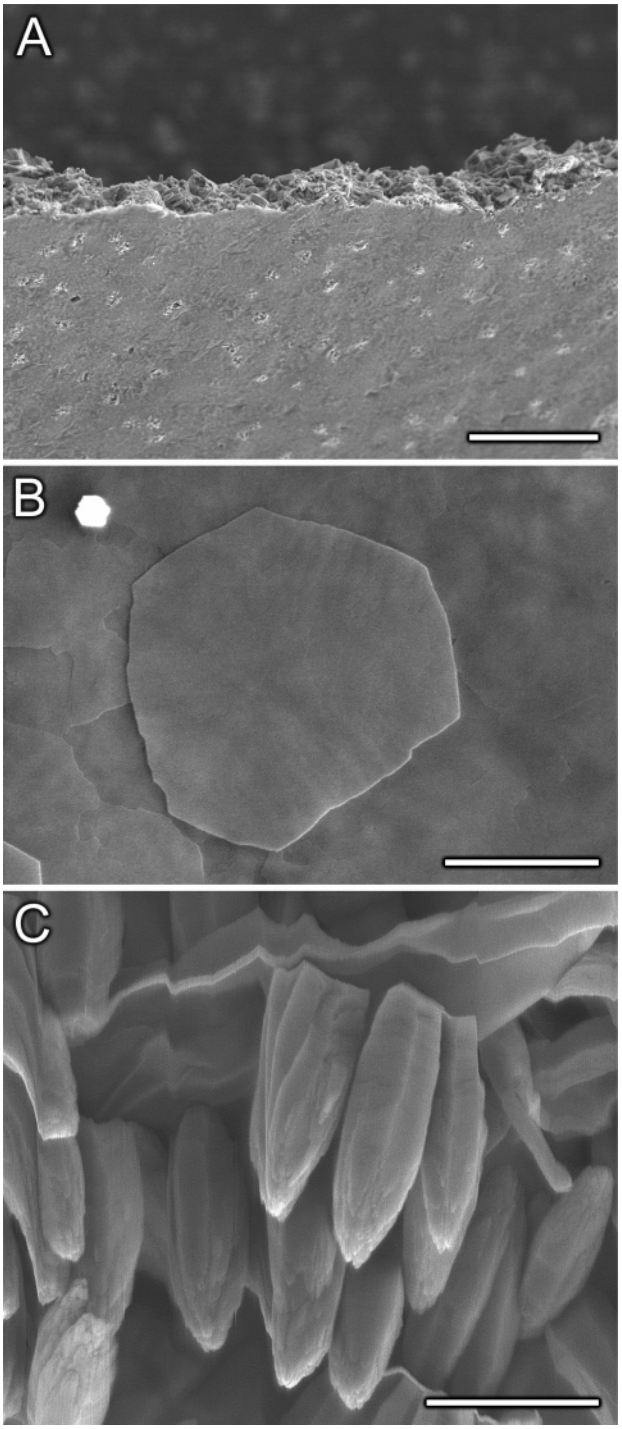

Figure 1. (a) SEM images depicting thick films formed from the hydrolysis and condensation of the zinc oxide precursor catalyzed by OH^- from ammonia diffusion. Scale bar = 10 μm. (b) Higher resolution image of the top of the film depicting thin platelets formed at the gas−liquid interface during the initial nucleation event. Scale bar = 1 μm. (c) High-magnification imaging of anisotropic crystals from the region indicated in the box in a growing down into the zinc nitrate solution. Scale bar = 1 μm.

corresponding to (10−10) ZnO. HR-TEM analysis of the fractal outgrowth regions shows more oriented (Figure 3c) ZnO nanocrystals with preferential alignment to one another. SADP analysis of a fractal region (upper right, Figure 3c) demonstrates the single-crystal-like nature of these growths, confirming observations shown in Figure 3c.

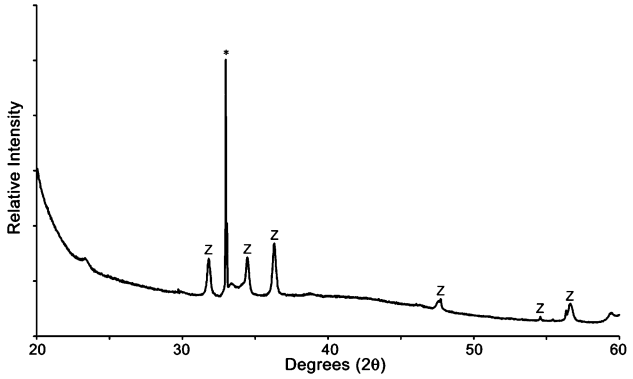

Figure 2. X-ray diffraction of the reaction product confirming the presence of crystalline ZnO (wurtzite phase, JCPDS#36-1451). Z indicates zinc oxide peaks, and * indicates Si peaks from the substrate.

To understand the formation of the ZnO platelets at the gas−liquid interface due to the spatially and temporally controlled increase in reagent concentration, the aqueous chemistry of zinc and its hydrolysis must be considered. Upon dissolution of a zinc salt (e.g., $Zn(NO_3)_2$) in water, Zn^{2+} cations become octahedrally coordinated to form the hexaqua ion, $Zn(OH_2)_6^{2+}$. Since the Zn^{2+} cation has a low valency and a relatively modest ionic radius (88 pm), its polarizing power (i.e., its ability to withdraw electron density) is relatively weak. Therefore, at low pH (∼1−5), hydrated zinc is quite stable. Using the partial charge model (PCM),[38] which allows estimation of the charge and identification of the molecular species of a cation at specific values of pH, we see that the hexaqua zinc species becomes destabilized with increasing pH due to its tendency to deprotonate and undergo hydrolysis

$$Zn(OH_2)_6 \rightarrow Zn(OH_2)_{6-h}(OH)_h \quad (1)$$

where h is the hydrolysis ratio.

At the pH of the starting 50 mM zinc nitrate solution (pH ≈ 5) the PCM predicts minimal hydrolysis (i.e., $h = 1.2$), predicting that the resulting majority species ($[Zn(OH_2)_5(OH)]^+$) will be stable against precipitation. However, as the OH^- concentration increases (e.g., at pH ≈ 7) the PCM predicts that an additional zinc-coordinated water molecule will deprotonate, leading to formation of a neutral, less soluble, hydrolyzed species (i.e., $h = 1.9$ or $\sim Zn(OH_2)_4(OH)_2$). This species can subsequently undergo condensation reactions via olation or oxolation with subsequent elimination of water. These condensation reactions progressively lead to the formation of an extended metal oxide (or hydroxide) network, the solubility of which is rapidly reduced, thereby initiating nucleation.

By measuring pH changes at the gas−liquid interface during the controlled diffusion of ammonia into the zinc-containing precursor solution we can identify the $[OH^-]$ changes concurrent with the formation of ZnO. For continuous pH measurement using the same experimental configuration used in the ZnO growth, we immersed a pH probe into a vessel containing MQ water. The probe was submerged 0.5 cm below the gas−liquid interface. A 50 mL beaker containing a dilute solution (0.28 wt %) of ammonia was then sealed ($t = 0$) in the desiccator

(38) Henry, M.; Jolivet, J. P.; Livage, J. In *Chemistry, Spectroscopy and Applications of Sol−Gel Glasses*; Reisfeld, R.; Springer-Verlag: New York, 1992; Vol. 77, p 153.

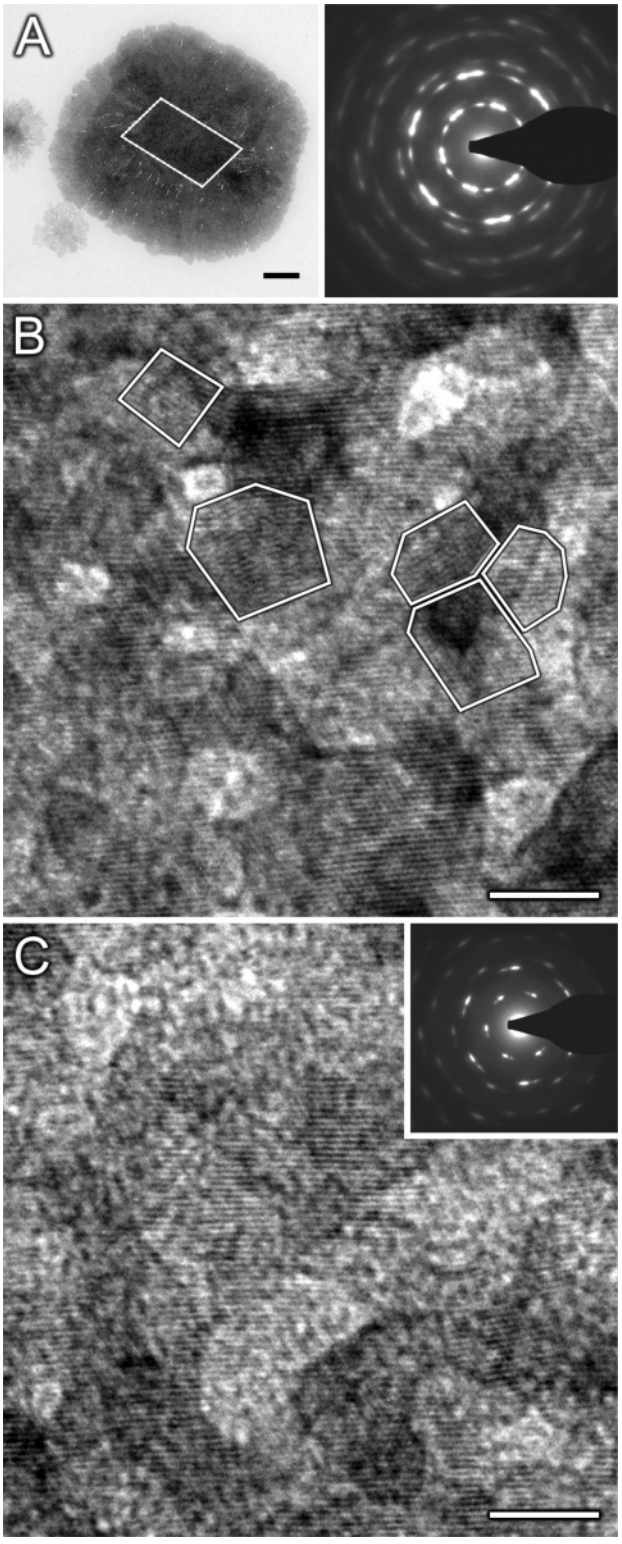

Figure 3. (a) TEM images of initial platelets formed at the gas−liquid interface consisting of a core-seed and fractal-like outgrowths. Scale bar = 200 nm. (Upper right, a) SADP of platelets along the [0001] axis indicating highly textured ZnO. (b) HR-TEM of the core region, highlighted in a, depicting ~3 nm crystallites oriented along the [0001] axis with random in-plane texturing. The *d* spacing of nanocrystals = 2.82 ± 0.03 Å corresponding to (01−10) ZnO. Scale bar = 5 nm. (c) HR-TEM of the fractal-like region showing the co-alignment of crystallites along the [01−10] direction. Scale bar = 5 nm. (Upper right, c) SADP of c along the [0001] axis indicating oriented ZnO.

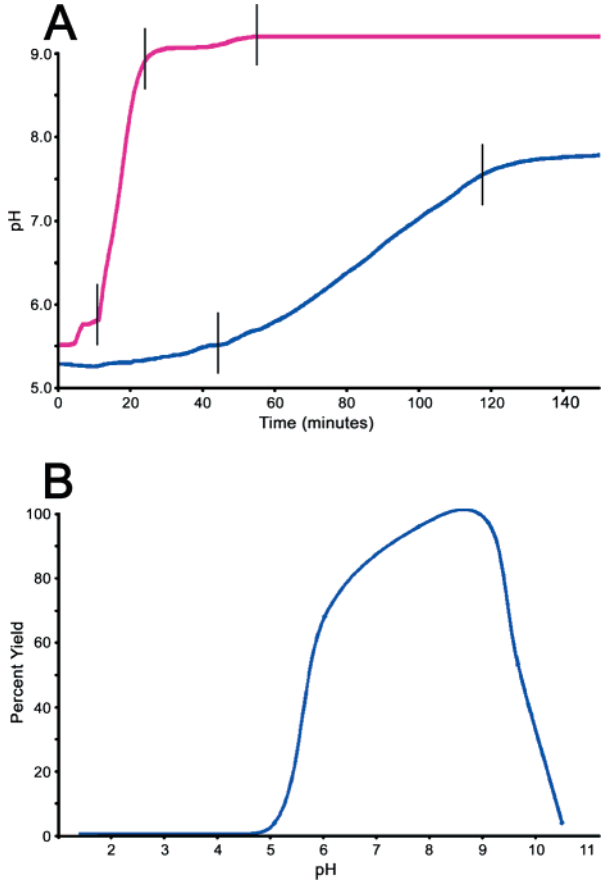

Figure 4. (a) Observations of pH as a function of time for ammonia diffusing into MQ water and 50 mM zinc nitrate. The reduced rate of pH change in the zinc nitrate solution is indicative of a lower diffusion coefficient of ammonia in the solid product versus that in water.[39] Demarkations in both plots denote induction, high flux, and equilibrated regions. (b) Yield of ZnO powder from the hydrolysis of zinc nitrate as a function of pH. Precipitation of ZnO is first seen at pH ≈ 6.8, in agreement with the PCM prediction of molecular species.

along with the pH-monitored MQ water. Figure 4a shows the observed time-dependent increase in pH (at a 0.5 cm depth) of MQ water and 50 mM zinc nitrate exposed to ammonia. The pH profile of MQ water exposed to ammonia is sigmoidal, with an induction period during which there is no change of pH in the water; this is most likely the period during which ammonia is saturating the desiccator chamber. However, after this short induction time, the ammonia diffuses to the probe, as indicated by the slow rise in pH. The rate of pH change is greatest once the flux of ammonia molecules into the water reaches a maximum and then slows and reaches a plateau, indicating that the entire system (desiccator, ammonia source, and water bath) has reached chemical equilibrium.

The same diffusion experiment performed with 50 mM zinc nitrate demonstrated a slightly different pH−time profile. The same induction and slow pH change periods are seen for both the precursor solution and the water, but upon reaching pH ≈ 7, the rate of change of pH in the precursor solution begins to decrease as evidenced by the shallower slope. It is during this period that the formation of ZnO platelets is observed. Finally, after a long period of time (e.g., 20 h) the system reaches chemical equilibrium. The rate of diffusion is closely related to the properties of the medium through which the molecules pass. For ammonia, the diffusivity, *D*, through liquid is 3−4

orders of magnitude greater than through a solid,[39] in agreement with data observed in Figure 4a.

Figure 4b compares the yield of ZnO powder as a function of pH for a dilute solution of ammonium hydroxide mixed with a dilute solution of zinc nitrate. It is clear from these data that the initial formation of stable nuclei of ZnO occurs at pH $\approx$ 6.8, in agreement with our observations in Figure 4a as well as with calculations from the PCM that predict the abundance of a significantly hydrolyzed species at pH = 7.

Since there is no surface upon which condensing species (embryonic nuclei) may form, precipitation is likely to occur at the gas−liquid interface (as seen in Figure 3a and b). The small size of these nuclei (ca. ∼3 nm) is an indication of their rapid formation due to a large driving force. In addition, since the chemical potential of the precursor solution can be assumed constant across the interface, more than one nucleation event must occur, as observed from the multiple nuclei in the core. These particles are oriented with the crystallographic *c* axis perpendicular to the gas−liquid interface. The growth direction of these platelets appears to be in the ⟨01−10⟩ direction, which is not the usually preferred growth direction.[40] The basal plane of ZnO (i.e., (0001)) usually exhibits the fastest growth velocity due to its high surface energy.[40] In the observations presented here, growth appears to begin along the ⟨01−10⟩ direction, corresponding to the nonpolar (01−10) face. This is most likely the result of a constraint on growth imposed by the lack of growth medium above the liquid surface and the large supply of nutrient in the direction perpendicular to the *c* axis. Growth does not initially occur downward into the solution (i.e., ⟨000−1⟩) due to the fact that (1) the greatest change in pH occurs radially to the growing seeds where OH^- can be most easily incorporated into the crystal and (2) the growth velocity of ZnO is typically lowest in the ⟨000−1⟩ direction.[40]

Subsequent formation of secondary nuclei seems to occur heterogeneously upon the core nanoparticles. This is reasonable since the activation barrier for nucleation is now significantly reduced due to the presence of a solid interface (i.e., the core seed). Additional growth of these plates continues radially in the high-pH regions close to the precursor solution surface through the accretion of oriented nanoparticles that now recognize the solid interface (Figure 3c). Formation of a solid at the gas−liquid interface must impede the subsequent diffusion of ammonia, as reflected in the reduced rate of pH change in zinc nitrate compared to that in MQ water. As the pH rises to reach a critical threshold beneath the surface of the core seed, additional nucleation and growth of ZnO occurs without chemical constraint (i.e., in the now homogeneous environment). Growth now occurs in the ⟨0001⟩ direction (Figure 1d), as predicted in a homogeneous environment.[40]

Under certain reaction conditions more soluble species such as $[Zn_5(OH)_8(NO_3)_2(OH_2)]$ or $Zn(OH)_2$ will initially form. These products have been observed as the initial phase during hydrolysis of aqueous zinc salts[26,33] and identified by XRD at very short reaction times (i.e., 1 h, data not shown) in our synthesis. However, with extended time and a reduced growth rate, pH changes (e.g., higher $[OH^-]$) will induce dissolution−reprecipitation reactions to form ZnO[41] (as confirmed by XRD) in a manner similar to other mineral systems.[42]

We demonstrated a unique method to produce ZnO films by a process inspired from biomineralization conditions that harnesses reagent diffusion for the kinetic control of precursor hydrolysis and subsequent crystal growth. Initial formation of textured nanoparticles at the gas−liquid interface occurs via homogeneous nucleation followed by aggregation. Subsequent nucleation and secondary growth occurs heterogeneously upon the initial seed templates in an oriented manner. Use of this slow diffusion method combined with prediction of molecular species using the PCM at a specific pH enables a higher level of organizational control than obtained in other low-temperature synthesis methods, without the use of organic molecules.[34] Various metal oxides and their morphologies and chemical compositions can also be tailored for specific applications using this relatively simple approach. Use of this technique for controlled synthesis of such materials is currently in progress. As foreseen by Heuer et al.,[1] we and others thus are beginning to incorporate the control principles utilized by nature into existing technologies via biomimetics and bioinspiration[1,16−19,43−45] in order to develop low-cost routes to high-purity metal oxide semiconducting materials with variable dimension and unique optoelectronic properties.

Acknowledgment. This work was supported by grants from the U.S. Department of Energy (DE-FG03-02ER46006), the Institute for Collaborative Biotechnologies through grant DAAD19-03-D-0004 from the U.S. Army Research Office, NASA (NAG1-01-003 and URETI-00000532), the NOAA National Sea Grant College Program, the U.S. Department of Commerce (NA36RG0537, Project R/MP-92) through the California Sea Grant College System, and the MRSEC Program of the National Science Foundation under award DMR-96-32716 to the UCSB Materials Research Laboratory.

JA062434L

(39) Bennett, C. O.; Myers, J. E. *Momentum, Heat, and Mass Transfer*, 3rd ed.; McGraw-Hill: New York, 1982.
(40) Li, W. J.; Shi, E. W.; Zhong, W. Z.; Yin, Z. W. *J. Cryst. Growth* **1999**, *203*, 186.
(41) Reichle, R. A.; McCurdy, K. G.; Hepler, L. G. *Can. J. Chem.* **1975**, *53*, 3841.
(42) Liu, H.; Wei, Y.; Sun, Y.; Wei, W. *Colloids Surf. A: Physiochem. Eng. Aspects* **2004**, *252*, 201.
(43) Sarikaya, M.; Aksay, I. A. E. *Biomimetics: Design and Processing of Materials*; American Institute of Physics Press: Williston, VT, 1995.
(44) Roth, K. M.; Zhou, Y.; Yang, W.; Morse, D. E. *J. Am. Chem. Soc.* **2005**, *127*, 325.
(45) Nam, K. T.; Kim, D. W.; Yoo, P. J.; Chiang, C. Y.; Meethong, N.; Hammond, P. T.; Chiang, Y. M.; Belcher, A. M. *Science* **2006**, *312*, 885.